Strongly Coupled Plasma Physics (S. Ichimaru, editor),
Elsevier Science Pub. B.V./Yamada Science Foundation,
pp. 189-200 (1990).

THEORY OF STRONGLY-CORRELATED PURE ION PLASMA IN PENNING TRAPS*

D. H. E. Dubin and T. M. O'Neil

Physics Department, Univ. of Calif. at San Diego, La Jolla, CA 92093 USA

1. INTRODUCTION

In a recent series of experiments[1] at the National Institute of Standards and Technology in Boulder, Colorado a cloud of ions is trapped and confined for long periods of time. The number of ions trapped, N, is sufficiently large so that the cloud may be regarded as a plasma, i.e., a nonneutral or pure ion plasma. The ions are subsequently cooled to extremely low temperature T at sufficiently high density n_0 so that the correlation parameter, $\Gamma = q^2/a_{ws}kT$ is much larger than unity (here q is the ion charge and $a_{ws} \equiv (3/(4\pi n_0))^{1/3}$ is the Wigner-Seitz radius). The ions therefore become strongly correlated and it is possible to study in detail the effects of strong correlation, including formation of liquid and even crystalline states. Furthermore, as we will see, there is a direct correspondence between the thermal equilibrium properties of these trapped ions and those of the so-called one-component plasma (OCP). All this is quite exciting since there is a large body of theoretical work which has been generated over several decades on the one-component plasma, and so it may be possible to test several of the theoretical predictions. For instance, it has been predicted that a first-order phase transition should occur from a liquid to a body-centered cubic (bcc) crystal at $\Gamma \cong 180$ in the infinite homogeneous OCP.[2]

Does this result apply to the experiments? We will see that in fact the result does not apply, because in present experiments the number of ions trapped is relatively small ($N \lesssim 10^4$) so that surface effects are important. However, because the number of ions is small, computer simulation of the system in realistic geometry becomes possible. We will discuss the results of such simulations,[3] which predict correlation behavior in the ion clouds which is quite different from that of the homogeneous one-component plasma. Rather than undergoing a simple first-order transition from a liquid to a bcc crystal, the system passes through an intermediate regime rather like the smectic phase of a liquid crystal, in which the ion cloud forms concentric spheroidal shells. Ions are confined to the shells but move randomly within each shell. At larger Γ values, this diffusion is suppressed and a distorted 2-D hexagonal lattice forms in each shell.

*Supported by NSF grant PHY87-06358, ONR Contract N00014-82-K-0621 and a grant of cpu time from the San Diego Supercomputer Center.

Some of these properties can be understood by means of a simple slab model of the ion cloud. This model will provide us with a simple first estimate for the size of system required before the results of the infinite homogeneous computer calculations should apply to the pure ion crystal.[4]

In Section 2 we discuss several important properties of nonneutral plasmas and consider the confinement characteristics of such plasmas when trapped in the so-called Penning trap used in the experiments. In Section 3 the results of computer simulations are discussed, and in Section 4 an analytic model is presented which is based on a finite-temperature slab geometry model of a bounded ion crystal.

2. THERMAL EQUILIBRIUM OF STRONGLY-CORRELATED NONNEUTRAL PLASMAS

Nonneutral plasmas, that is, plasmas consisting of an unneutralized collection of charged particles, have many properties in common with neutral plasmas. For instance, they exhibit the phenomenon of Debye shielding and also exhibit collective effects such as plasma oscillations. However, there are several differences between neutral and nonneutral plasmas. For instance, when a nonneutral plasma is cooled to low temperature it suffers no recombination since there is no oppositely charged species with which to recombine. (We will focus here on single-species nonneutral plasmas—the experiments at NIST usually involve plasmas consisting of Be^+ ions.) At sufficiently low temperature and high density, the kinetic energy per particle is less than the interaction energy and the plasma becomes strongly correlated.

Another difference between the neutral and nonneutral plasma is that nonneutral plasmas can be confined for very long periods of time using only static electric and magnetic fields. In the experiments long-time confinement is provided by means of the cylindrical Penning trap geometry shown schematically in Figure 1. This trap in its simplest form consists of three electrically isolated conducting cylinders whose axes of symmetry are oriented parallel to a uniform magnetic field. Confinement in the axial direction is provided by a potential well induced by a voltage difference between the central cylinder and the end cylinders. Confinement in the radial direction is provided by the uniform magnetic field **B**. The radial confinement can be understood by analyzing the balance of forces in the radial direction. There is a large radial electric field E_ρ due to the unneutralized collection of ions in the trap. This electric field is balanced by the magnetic component of the Lorentz force,

$$E_\rho + \frac{v_\theta B}{c} \cong 0 \quad , \tag{1}$$

where v_θ is the velocity of the particles in the azimuthal direction. Solving for the velocity v_θ, we find that the entire plasma rotates about the axis of symmetry. This rotation is just the familiar $E \times B$ drift.

Another way to understand the radial confinement of the nonneutral plasma is to consider the constants of the motion. Cylindrical symmetry implies that the total angular momentum in the axial direction is a constant of the motion:

$$L = \sum_i (m v_{\theta i} + \frac{q}{c} A_\theta(\rho_i)) \rho_i \quad , \tag{2}$$

where $A_\theta(\rho) = B\rho/2$ is the vector potential associated with the magnetic field. If the magnetic field is sufficiently strong the vector potential contribution to the angular momentum dominates over the kinetic contribution and the angular momentum can be written in the following form:

$$L \equiv \frac{qB}{2c} \sum_i \rho_i^2 \quad . \tag{3}$$

This equation implies that the mean square radius of the plasma is a constant of the motion and thus the plasma cannot expand. This simple argument has been made more rigorous by O'Neil.[5] In the actual experiments small imperfections in the trap cause slight cylindrical asymmetries which allow the plasma to slowly expand. However, by careful construction, these asymmetries can be reduced and confinement times on the order of several days have been achieved in experiments on pure electron plasmas at the University of California in San Diego.[6]

These confinement times are much longer than any internal time scales in the dynamics and so the particles can come to a state of confined thermal equilibrium. The thermal equilibrium is characterized by the angular momentum L and the energy H, where

$$H = \sum_{i=1}^{N} \frac{1}{2} m v_i^2 + e\Phi(\mathbf{x}_1, \cdots \mathbf{x}_N) \tag{4}$$

and Φ is the potential energy of the system of charges, including electrostatic interactions and external confining potentials. If one then assumes that the system is thermally isolated, a microcanonical (constant H and L) ensemble describes the statistics of the system. However, it is often useful to use a canonical ensemble based on constant temperature T and rotation frequency ω. For large N the two ensembles predict averages which differ only $O(1/N)$. Such differences are unimportant for the N values considered here even though we are interested in effects stemming from the boundedness of the cloud. The probability density associated with a given state is then given by the Gibb's distribution f, where

$$f(\mathbf{x}_1, \mathbf{v}_1, \cdots \mathbf{x}_N, \mathbf{v}_N) = Z^{-1} e^{-\beta(H + \omega L)} \quad . \tag{5}$$

For given external confining fields N, f is characterized by the parameters T and ω and these parameters in turn determine the average values of the energy and angular momentum of the system. Substituting Eq. (2) and (4) into Eq. (5) yields, after some simple algebra, the following form for f:

$$f = Z^{-1} e^{-\beta m \sum_i (v_i - \omega\rho_i\hat{\theta}_i)^2/2} \times e^{-\beta(\Phi + \sum_i \frac{m\omega}{2}(\Omega_c - \omega)\rho_i^2)} \tag{6}$$

One can see that the velocity dependence is Maxwellian in a frame rotating with frequency ω. As one expects, the thermal equilibrium distribution corresponds to a shear free flow. We call such a flow a rigid rotor.

In Eq. (6), the spatial distribution of ions is determined by three potentials: the total electrostatic potential Φ, the centrifugal potential $-m\omega^2\rho^2/2$ and the potential $m\omega\Omega_c\rho^2/2$. This

latter potential is associated with the electric field induced by rotation through a magnetic field. It is this field that provides the radial confinement. It dominates over the deconfining effect of the centrifugal potential, since the cyclotron frequency is larger than the rotation frequency in the experiments. These two potentials form an effective potential which is proportional to ρ^2 and thus they can be interpreted as the potential energy of ions in a cylinder of uniform negative charge. The density of this effective neutralizing background charge n_0 may be found by substituting the effective potential into Poisson's equation:

$$n_0 = \frac{\nabla^2}{4\pi q^2}\frac{m\omega}{2}(\Omega_c - \omega)\rho^2 = \frac{m\omega(\Omega_c - \omega)}{2\pi q^2} \quad . \tag{7}$$

Thus, the static thermal equilibrium properties of the magnetically confined plasma are the same as those of a one-component plasma, that is, a system of charges embedded in a uniform neutralizing background charge. This OCP resides in the potential well that is produced by the cylinder of uniform neutralizing charge and the end electrodes. For given potentials on the end electrodes and a given value of $\omega(\Omega_c - \omega)$ one can determine the shape of this confining potential well. Of course, the shape of this well is important in determining the shape of the plasma. For the simple case of a small plasma at the bottom of the well the effective confining potential is approximately quadratic and can be written as

$$\Phi_{conf} = \frac{m\omega_z^2}{2}(z^2 + \alpha\rho^2) \tag{8a}$$

where ω_z is the single-particle axial bounce frequency in the external trap potential, and

$$\alpha = \frac{\omega(\Omega_c - \omega)}{\omega_z^2} - \frac{1}{2} \tag{8b}$$

is the "trap parameter" which determines the shape of the effective confining potential. For this case Bollinger[7] and Turner[8] have shown that the plasma takes the shape of an ellipsoid as $T \to 0$, neglecting correlation effects. Correlations between charged particles in the plasma then are set up within this overall shape.

The correlation properties of strongly correlated one-component plasmas have been the subject of several theoretical investigations. Computer simulations of unbounded homogeneous one-component plasmas predict that for $\Gamma \geq 2$ the system begins to exhibit the local order characteristic of a liquid and for $\Gamma \sim 180$ there is a phase transition to a bcc crystal.[2] Current experiments with cryogenic pure ion plasmas in a Penning trap have achieved Γ values in the range of several hundred, but the experiments involve a relatively small number of particles so the theoretical studies of an infinite homogeneous one-component plasma cannot be trusted. On the other hand, these small plasmas are ideally suited for numerical simulations with a realistic number of particles. In order to study the correlation properties of these bounded plasmas we have carried out molecular dynamic (MD) simulations and Monte Carlo (MC) calculations with boundary conditions motivated by the experiments.

In the MD simulation, the equations of motion for N interacting charges in a Penning trap are integrated forward in time until the charges come into thermal equilibrium with each other. Average properties of the system such as the local density $n(\mathbf{x})$ are then determined as long-time averages: for instance,

$$n(\mathbf{x}) = \sum_{i=1}^{N} \int_0^{\tau} \frac{dt}{\tau} \delta(\mathbf{x} - \mathbf{x}_i(t)) \quad .$$

In contrast, the MC calculation is a statistical game of chance based on the distribution for a canonical ensemble. We find that the MD simulation and the MC calculation yield the same answer for average quantities such as the local density, provided that $N \gtrsim 100$ within the statistical error of the simulations. This is in general agreement with the previously stated result that the canonical and microcanonical ensembles yield the same average properties for large N.

There is one subtlety which should be noted in our molecular dynamics simulations. In the experiments the cyclotron radius typically is much smaller than the distance between particles, or equivalently, the cyclotron period is much shorter than an interaction time. Under these circumstances it is useful to average out the high frequency cyclotron dynamics before turning to the computer. This is accomplished by using the guiding center equations of motion rather than the exact equations of motion. Although the guiding center equations are only approximate, the thermal equilibrium structure obtained with them is not. By substituting the guiding center Hamiltonian and guiding center angular momentum into the Gibbs distribution (see Ref. 3), one finds the guiding center system has the same thermal equilibrium structure as the exact system for a slightly shifted magnetic field strength.

What follows are numerical results for the case of a small plasma at the bottom of the effective potential well given by Eq. (8).

3. NUMERICAL RESULTS

For convenience in displaying results, we typically choose conditions so that the well and plasma have spherical symmetry. The fact that the plasma radius is small compared to the radius of the conducting cylinder also implies that the force due to an image charge is small, so we take the interaction potential to be simply $e^2/|\mathbf{x}_i - \mathbf{x}_j|$. For the molecular dynamics simulation the guiding center equations of motion are solved using the fourth order Runga-Kutta algorithm and a fourth-order corrector algorithm, both with a variable time step. The codes have been tested against one another and have been vectorized to run efficiently on a CRAY X-MP computer. In the code, times are normalized to ω_z^{-1} and distances to $a_0 \equiv (3q^2/m\omega_z^2)^{1/3}$. [From Eqs. (7) and (8b), $a_0 = (2\alpha+1)^{1/3} a_{ws}$.] We typically integrate for times of order $10^4\,\omega_z^{-1}$, and in all cases energy is conserved to better than 1% of the total kinetic energy, and angular momentum to one part in 10^5. The MC calculation follows a standard Metropolis-Rosenbluth algorithm. Figure 2 shows the results of a MC calculation for Γ values ranging from 1 to 10. The average density $n(r)$ is plotted as a function of the spherical radius r for r values near the plasma edge. The effective potential well and plasma have spherical symmetry. For $\Gamma = 1$ the

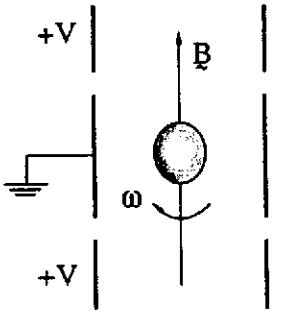

FIGURE 1
Cylindrical Penning Trap

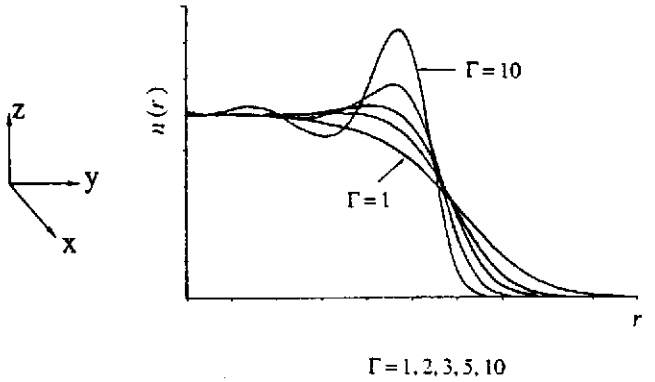

FIGURE 2
MC results for density at the edge of a trapped cloud for various values of Γ.

density falls smoothly to zero, as it does for weak correlation, but for higher values of Γ oscillations are present near the plasma edge. These oscillations are evidence of local order. The damping length for the oscillations is a measure of the correlation length. One may think of the density maxima as embryonic lattice planes or more precisely spherical lattice shells. Such oscillations have also been observed in previous Monte Carlo studies of the so-called one-component plasma with an edge,[9] and were also observed by Totsuji for trapped ions.[10] Schiffer has also studied the correlation properties of cold ion clouds trapped in heavy ion storage rings.[3]

As Γ is increased, the oscillations increase in magnitude until the density between peaks goes to zero. For a spherical cloud with 100 particles, this occurs at $\Gamma \sim 140$ (Fig. 3). Thus the ion cloud separates into concentric spheres. For $N = 100$ there are three spheres with four ions in the innermost sphere, 26 in the middle sphere, and 70 in the outermost sphere. The areas under each peak are about equal implying that the number of ions per unit area in each sphere is the same, being set by the background density n_0. Thus the number of ions per sphere roughly scales as the surface area of the sphere.

If one tags an individual particle on one of these shells, one finds that the particle is localized to the shell, but is not localized on the shell. For this value of Γ, the particles still diffuse over the surface of the shell, that is, the system behaves like a crystal in the radial direction but like a liquid along the surface of the shell as in a smectic liquid crystal. For the $\Gamma = 140$ and $N = 100$ case of Figure 3 we study the particle diffusion further by considering the mean square displacement of the ions in time. For instance, we determine the average of $\delta z^2(t)$ where

$$<\delta z^2>(t) = \frac{1}{mN} \sum_{i=1}^{N} \sum_{j=1}^{m} [z_i(t_j + t) - z_i(t_j)]^2 ,$$

and $t_j - t_{j-1}$ is a constant time increment and $t \leq t_j - t_{j-1}$. This function increases linearly in

time for $<\delta z^2>^{1/2}$ small compared to the cloud radius, so that we may obtain the average diffusion coefficient in the z direction, D_z, through the definition $<\delta z^2(t)>=2D_z t$. For $\Gamma=140$ this diffusion is shown in Figure 4 and may be contrasted to a similar plot of $<\delta r^2>$ in the same figure, where r is the spherical radius from the center of the cloud. While $<\delta z^2>$ does indeed increase linearly with time, $<\delta r^2>$ is almost constant, showing that there is little diffusion of ions from sphere to sphere.

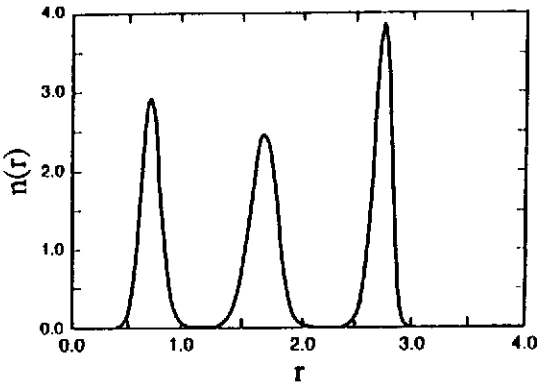

FIGURE 3
MD result for density of a cloud with $\alpha=1$, $N=100$, $\Gamma=140$.

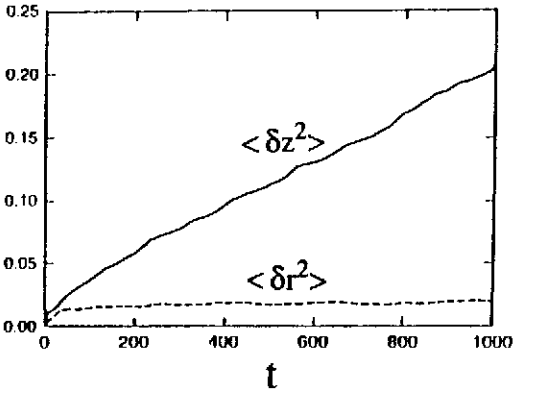

FIGURE 4
Diffusion in r and z for ions in cloud of Fig. 3; $\omega_z/\Omega_c=0.1$.

For substantially higher values of Γ the particle diffusion along the surface of a shell also goes to zero and an imperfect 2-D hexagonal crystal is formed on the shell. Figure 5 shows a projection onto a plane of one-half of the outer shell for a $N=256$ spherical plasma. For $\Gamma\gtrsim 380$, the ions were confined to the lattice sites shown; the sites form a local equilibrium which may be thought of loosely as going to the $T=0$ or $\Gamma=\infty$ limit. However, one should note that there are many such local equilibria in the N particle potential energy. Nevertheless there is a tendency toward a hexagonal crystal which one can identify in Figure 5. One may confirm this intuition by calculating the spatial correlation $c(s)$ function of all ions within a particular sphere. This function is defined as the probability density that an ion is at a distance s from another ion, counting only ions on a given shell. For $\Gamma=140$ this correlation displays decaying oscillations characteristic of a fluid. However, for larger values of Γ the correlations become more highly peaked and the peaks correspond in position to those of a 2-D hexagonal crystal, and furthermore the number of ions in each peak correspond to that expected for 2-D hexagonal symmetry (see Fig. 6).

Another useful correlation function which further characterizes the crystalline order is the bond angle correlations $c_\theta(\theta)$ in the shell. This correlation function is defined as a probability density that a bond angle is at angle θ, averaged over all ions in a shell. The set of bond

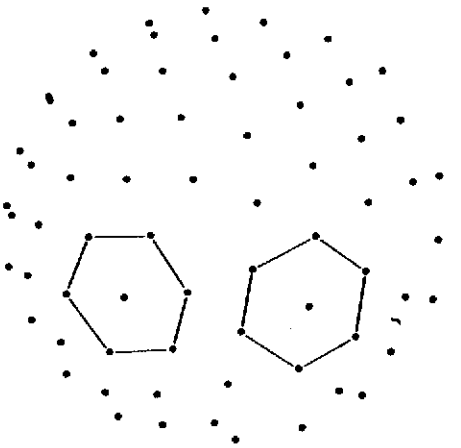

FIGURE 5
$T=0$ equilibrium state for 1/2 of outer shell of an $N=256$ spherical cloud.

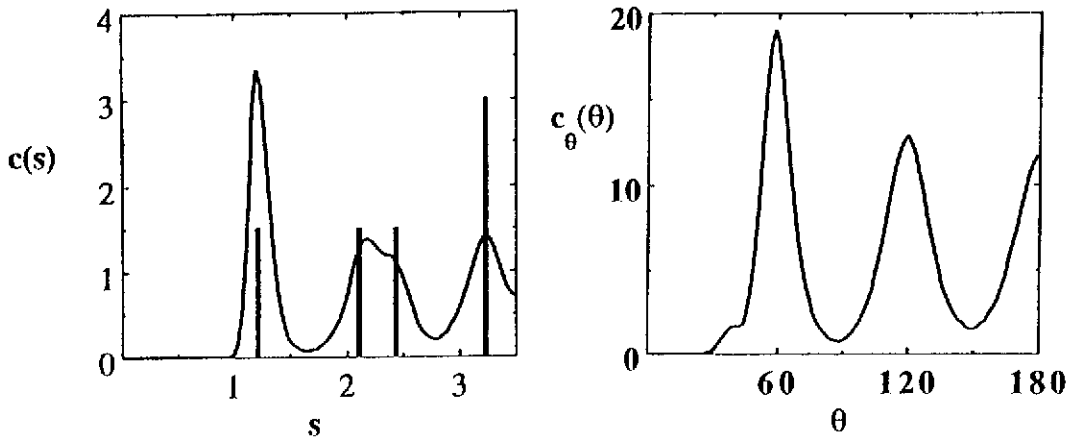

FIGURE 6
Correlations within outer shell of $N=256$ cloud at $\Gamma=380$. a) Spatial correlations. Vertical lines give positions and weights for $T=0$ 2-D hexagonal lattice; b) Bond angle correlations, using 6 nearest neighbors in shell.

angles for a given ion are those angles subtended by any two of the ion's M nearest neighbors, using the given ion as a vertex; there are $M(M-1)/2$ such angles for each ion. As plotted in Figure 6 for the case of the outer shell of the $N=256$, $\Gamma=380$ crystallized cloud, one sees that the bond angle correlation function corresponds well to that expected for a 2-D hexagonal lattice.

This lattice structure is quite different from the bcc lattice predicted for an infinite homogeneous one-component crystal. Indeed, if one determines the three-dimensional spatial correlation function within a large Γ cloud one finds that even for large N the correlations bear little

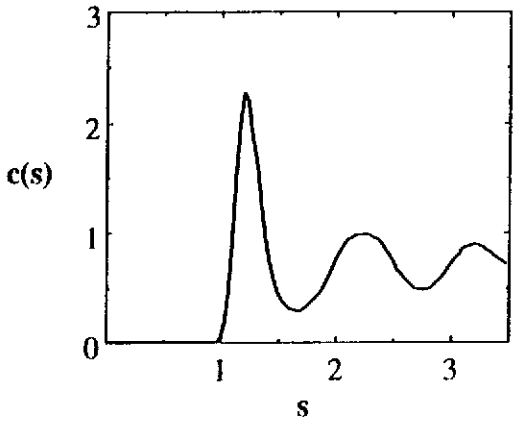

FIGURE 7a
3-D spatial correlations in $N = 2048$, $\alpha = 1$, $\Gamma = 290$ cloud, counting ions only within $r < 4.8$ (cloud extends to $r = 8$). First peak contains 14 ions.

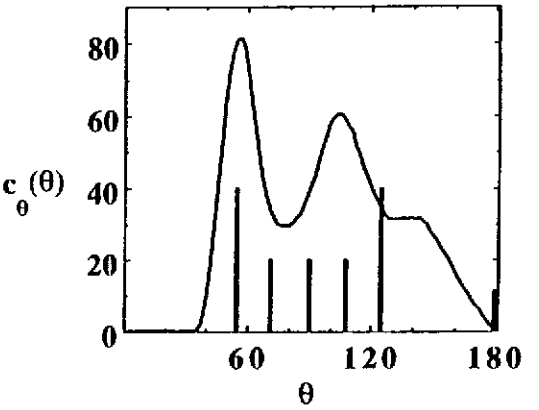

FIGURE 7b
3-D bond angle correlations for $N = 256$ $\Gamma = 380$ cloud, using 14 nearest neighbors in cloud for each ion within inner shells. Vertical lines are $T = 0$ bcc lattice bond angles (14 n.n.).

resemblance to those of a body-centered cubic crystal. The three-dimensional bond angle correlations are also quite different (see Fig. 7).

We have performed computer simulations for up to 2,048 ions and we observe no convincing evidence of a body-centered cubic structure in the bulk of the ion clouds. Presumably, however, as $N \to \infty$, the system becomes infinite and homogeneous and the body-centered cubic crystal structure should appear. So the question arises, how large must an ion cloud be before this bulk behavior is observed?

4. SLAB MODEL OF THE BOUNDED COULOMB SYSTEM

In this section we consider in more detail how the boundedness of an ion system can affect its lattice structure. In the process, an estimate is obtained for the size of system required before infinite volume behavior is achieved, and several other relations are derived, including the approximate spacing between shells in the ion clouds, a result which can be compared to numerical and experimental results.

In order to make theoretical progress we consider a slab model of a bounded Coulomb crystal, which neglects the effect of curvature but still incorporates the effects of boundedness. The model consists of a collection of ions trapped in planar geometry in a 1-D quadratic well of the form $m\omega_0^2 z^2/2$. Note that this potential is that due to a uniform density background (here $n_0 = m\omega_0^2/(4\pi q^2)$), so this system is an OCP. The system is infinite and homogeneous in the x–y plane but bounded in the z-direction. This model allows us to make predictions concerning the lattice structure of ion clouds which are large enough so that shell curvature is small compared to the inter-ion spacing.

We find that the $T = 0$ equilibria for this system consist of a series of 2-D lattice planes

oriented parallel to the $x-y$ plane. Sufficiently far into the bulk from the surfaces, these planes become evenly spaced in z, setting up a 3-D bulk lattice (see Fig. 8). The free energy F of this system then depends on the density n_0, the total number of ions per unit $x-y$ area $\overline{\sigma}$, the temperature T, the type of 3-D bulk lattice (e.g. bcc, fcc, hcp, etc.) and the orientation of the bulk lattice with respect to the surfaces. These latter two thermodynamic parameters are written in the language of solid state physicists by stating which bulk lattice plane lies parallel to the surface; for instance an fcc(111) lattice is the bounded lattice consisting of an fcc lattice in the bulk with the (111) plane oriented parallel to the surface.

In general the thermodynamically stable state is that which has minimum free energy. The free energy per ion F can be written as a sum of bulk and surface terms:

$$F = F_b + 2F_s/P \tag{9}$$

where F_b is the free energy per ion of the bulk lattice (including the "Vlasov" energy per ion of a uniform slab of charge in the external quadratic well), P is the number of lattice planes in the system (a function of $\overline{\sigma}$ and the lattice type), and F_s is the (positive) surface free energy. For a given T, n_0, and lattice type, as $\overline{\sigma}$ approaches infinity the number of planes P also approaches infinity, and by Eq. (9) $F \to F_{bulk}$. In this limit the system becomes infinite and homogeneous and, as is well known, the lattice with minimum free energy is body-centered cubic (bcc). However, for finite P surface effects are important; ion-ion correlations in the z direction are disrupted by the finite system size and bcc symmetry in the bulk is no longer necessarily the minimum free energy state.

We have determined F for this system as a function of $\overline{\sigma} n_0^{2/3}$ and Γ for various lattice types and orientations, in the "harmonic approximation," in which the temperature is assumed to be sufficiently small so that ions move only slightly from their lattice sites and the interion force may then be linearized (i.e., the system is assumed to be an ideal gas of phonons). Anharmonic effects, which are important near the liquid-solid phase transition, have not yet been included. In this approximation the free energy per ion may be written as

$$F = \phi_v + E_{corr} + \frac{kT}{N}\sum_{r=1}^{3N-3} \ln\left[\frac{\omega_r}{\omega_0}\right] + 3kT \ln\left[\frac{\hbar\omega_0}{kT}\right] \tag{10}$$

where $E_{corr} = E_b + 2E_s/P$ is the $T=0$ electrostatic correlation energy per ion. Here, E_b is the correlation energy per ion of the infinite homogeneous lattice and E_s is the contribution to the energy due to the two surfaces. The "Vlasov energy" ϕ_v gives the energy per ion of a uniform slab of charge in the quadratic well; E_{corr} is the additional energy due to the fact that the slab is actually made up of lattice planes.[4] The frequencies ω_r are the normal mode frequencies of the bounded lattice; the sum over normal modes may be interpreted for $N \to \infty$ as an average over the reciprocal cell of the lattice, and is written as $\frac{1}{N}\sum_r \ln(\omega_r/\omega_0) \equiv \langle \ln(\omega_r/\omega_0)\rangle$. This average approaches a constant "bulk" value as $P \to \infty$; the remainder for finite P is a surface term, which may be written as $\langle \ln(\omega_r/\omega_0)\rangle = \langle \ln(\omega_r/\omega_0)\rangle_b + 2\langle \ln(\omega_r/\omega_0)\rangle_s/P$. Comparison

of Eqs. (9) and (10) then lead to the following identification for F_b and F_s:

$$F_b = \Phi_v + E_b + 3kT \ln\left(\frac{\hbar\omega_0}{kT}\right) + kT \langle \ln(\omega_r/\omega_0)\rangle_b \quad ,$$

$$F_s = E_s + kT \langle \ln(\omega_r/\omega_z)\rangle_s$$

We have determined E_b, E_s, $\langle \ln(\omega_r/\omega_0)\rangle_b$ and $\langle \ln(\omega_r/\omega_0)\rangle_s$ for various lattices. The values of E_b for bcc, hcp and fcc lattices are well-known, and $\langle \ln(\omega_r/\omega_0)\rangle_b$ has been determined for the bcc lattice.[2] (A previously-published value for the fcc lattice [11] is incorrect due to numerical error.) Values for E_b and E_s are found in Ref. 4 for these lattices as well as for other lattices, and we include in Table 1 some of our results for $\langle \ln(\omega_r/\omega_z)\rangle_b$ and $\langle \ln(\omega_r/\omega_z)\rangle_s$. Details of this calculation will appear elsewhere.

These results allow us to compare the free energy of the various lattice types as a function of $\bar{\sigma} n_0^{2/3}$ and Γ. We find that for $\bar{\sigma} n_0^{2/3} \gtrsim 53$ (corresponding to about 60 bcc(110) planes), the minimum free energy lattice always has bcc(110) symmetry, regardless of Γ. However for $\bar{\sigma} n_0^{2/3}$ below this value, a competition occurs between the fcc(111) and bcc(110) lattices; the winner is usually fcc(111). (The rather complex phase diagram is shown in Fig. (9). Precise details of the diagram in the small Γ region should not be taken too seriously since our free energies neglect anharmonic effects. However, the general structure—bands of alternating fcc

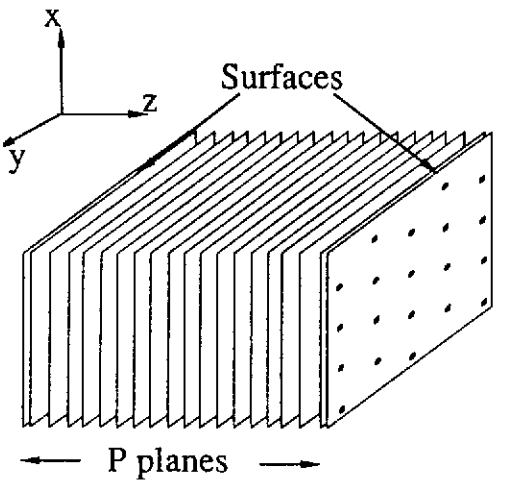

FIGURE 8
Schematic of $T = 0$ ion slab equilibrium for 20 planes.

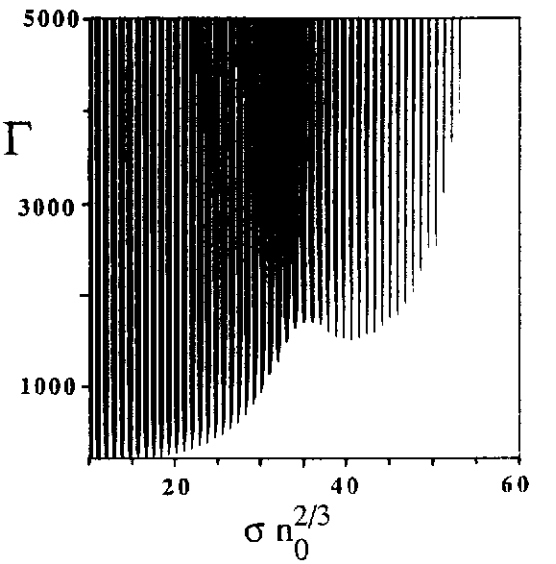

FIGURE 9
Phase diagram for bounded ion slab in regime $200 < \Gamma < 5000$, $10 < \bar{\sigma} n_0^{2/3} < 60$. fcc (111) lattice has lower free energy than bcc (110) in dark region.

Table 1

lattice type	$<ln(\omega_r/\omega_0)>_b$	$<\ln(\omega_r/\omega_0)>_s$
fcc (001)	-2.45373(1)	0.105(1)
fcc (111)	-2.45373(1)	0.240(2)
bcc (001)	-2.49384(1)	-0.20(1)
bcc (110)	-2.49384(1)	0.233(1)

and bcc symmetry—is probably correct. It should also be noted that for large Γ metastable equilibria may exist for long times before thermodynamic equilibrium is achieved.) The dominant fcc structure may be understood through the fact that fcc(111) lattice planes are 2-D hexagonal lattices, which is the most efficient 2-D packing method, so planes are spaced far apart and correlations between planes are minimized. Surface effects, which raise F, depend on interplane correlations and are therefore also minimized. These surface effects are important even for large $\overline{\sigma}$ because F_b is almost the same for fcc and bcc lattices, so only small differences in F_s are needed to affect the lattice structure.

Note that in the simulations a distorted 2-D hexagonal lattice also appears on each shell. The distance D between (111) planes in the fcc lattice is, for $\overline{\sigma}$ large and $T=0$, given by $Dn_0^{1/3} = 2^{2/3}/\sqrt{3} = 0.9165$, which corresponds closely to the numerical results, which give slightly larger values, of approximately .92 - .93 (see Fig. 3). However, the spheroidal shells are not as closely correlated as are fcc(111) planes (see Fig. 7). This is because shell curvature causes a loss of correlation from shell to shell since 2-D lattices on different shells get "out of phase" as one moves from point to point on the shell surfaces. If one entirely neglects correlations between shells one finds[4] that for large clouds the intershell distance is now $Dn_0^{1/3} = 0.956$; the intrashell lattice remains 2-D hexagonal. The simulation results lie between no intershell correlation and perfect fcc(111) correlation.

REFERENCES

1) S. Gilbert, J. Bollinger and D. Wineland, Phys. Rev. Lett. **60** (1988) 2022.
2) E. Pollock and J. Hansen, Phys. Rev. A **8** (1973) 3110; W. Slattery, G. Doolen and H. DeWitt, ibid. **26** (1982) 2255; S. Ogata and S. Ichimaru, ibid. **36** (1987) 5451.
3) D. Dubin and T. O'Neil, Phys. Rev. Lett. **60** (1988) 511; J. Schiffer, ibid. **61** (1988) 1843.
4) D. Dubin, Phys. Rev. A **40** (1989) 1140.
5) T.M. O'Neil, Phys. Fluids **23** (1980) 2216.
6) J. Malmberg et al., *Proc. of 1984 Sendai Symposium on Plasma Nonlinear Phenomena* (1984) 31.
7) J. Bollinger and D. Wineland, Phys. Rev. Lett. **53** (1984) 348.
8) L. Turner, Phys. Fluids **30** (1987) 3196.
9) See, for example, S. Ichimaru, H. Iyetomi and S. Tanaka, Phys. Rep. **149** (1987) 91.
10) H. Totsuji, Static and dynamic properties of strongly-coupled classical one-component plasmas: Numerical experiments on supercooled liquid state and simulation of ion plasma in the Penning trap, in: *Strongly Coupled Plasma Physics*, eds. F. Rogers and H. Dewitt (Plenum, New York, 1987) p. 19.
11) H. Helfer, R. McCrory and H. Van Horn, J. Stat. Phys. **37** (1984) 577.